Full Quantum Trajectories Resolved High-Order Harmonic Generation

Peng Ye, Xinkui He, Hao Teng,* Minjie Zhan, Shiyang Zhong, Wei Zhang, Lifeng Wang, and Zhiyi Wei†
Beijing National Laboratory for Condensed Matter Physics, Institute of Physics, Chinese Academy of Sciences, Beijing 100190, China
(Received 27 October 2013; published 13 August 2014)

We use a carrier-envelope-phase stabilized sub-2-cycle laser pulse to generate high-order harmonics and study how the two-dimensional spectrum of harmonics, with the resolutions in temporal frequency and spatial frequency, is shaped by the laser phase. An arrowlike spectrum obtained experimentally when the gas cell is located in front of the laser focus point shows a resolution of full quantum trajectories; i.e., harmonics from different trajectories stand on different positions in this spectrum. In particular, due to the laser phase combined with the classical-like action, the harmonics from short and long trajectories differ maximally in their curvatures of wave fronts in the generation area, and so occupy very different ranges of spatial frequency at the far field. The result directly gives a full map of quantum trajectories in high-order harmonic generation. The conclusion is supported by an analytical model and quantum mechanics simulations.

DOI: 10.1103/PhysRevLett.113.073601 PACS numbers: 42.50.Hz, 32.80.Rm, 42.65.Ky, 42.65.Re

High-order harmonic generation (HHG) from the extreme nonlinear interaction between femtosecond laser pulses and gas targets is an important method for providing an attosecond pulse source [1–3] and simultaneously a coherent extreme ultraviolet source [4]. The physical origin of HHG can be well described by a semiclassical three-step model [5]. The model is further developed to a full quantum mechanics description [6] and can be incorporated into the frame of Feynman's path integral theory [7,8]. In the frame, for each quantum trajectory the electron tunnels through the Coulomb barrier depressed by the laser field, then is accelerated in the laser field and spends time τ in the continuum, and finally recollides with the atomic core and generates harmonic with certain photon energy. Many trajectories in one half-cycle of the driven laser together compose a bundle of quantum trajectories. In each bundle the harmonic with the highest photon energy comes from the trajectory along which the electron spends time τ_c in the continuum. Quantum trajectories with a time τ less than τ_c are called short trajectories and those with τ larger than τ_c are called long trajectories.

Each quantum trajectory carries a specific part of the information of the whole process of HHG, such as the temporal-spatial distribution of the driven laser, the structure of the medium, and the dynamics of the medium. The information is transferred to high-order harmonics through the process of recollision, and makes the harmonics have different spatial-temporal properties that can be separated. If the harmonics form different quantum trajectories can be separated directly in the spectrum, it is convenient to obtain clues about the generation process to improve high-harmonic spectroscopy [9,10] and to study electron dynamics [11].

A full resolution of quantum trajectories requires two processes: generation and separation. Generation means that harmonics from all quantum trajectories can be generated and recorded. Separation means that, in the recorded spectrum, harmonics from different quantum trajectories locate at different positions. Some previous works have been done on this topic [12–14]. The amplitude of a few-cycle pulse varies dramatically from one half-cycle to another, so harmonics from different half-cycles occupy different ranges of temporal frequency. Haworth *et al.* [12] first experimentally observed high-harmonics emission, where short trajectories dominated, from each half-cycle. In one half-cycle, the harmonics come from short and long trajectories, along which the electron spends different times in the continuum and so emits harmonics with different ranges of spatial frequency [13–15].

This Letter presents studies on the two-dimensional high-order harmonics spectrum, with the resolutions in spatial frequency and temporal frequency, or conventionally speaking, in radiation angle and photon energy. The total phase of high harmonic is composed of the laser phase and the classical-like action. Radial distribution of the laser phase varies at different positions relative to the focus point, and together with the classical-like action leads to different shapes of the spectrum at the far field. When the gas cell is in front of the focus point, an arrowlike spectrum is obtained, as in Fig. 1. In this spectrum, harmonics from different quantum trajectories are separated. To our knowledge, it is the first time people can resolve full quantum trajectories, different bundles from different half-cycles and different trajectories in one bundle, directly in one spectrum. Our work reveals that, by using the proper laser phase, the wave front's curvatures of harmonics from the short and long trajectories differ maximally, so the

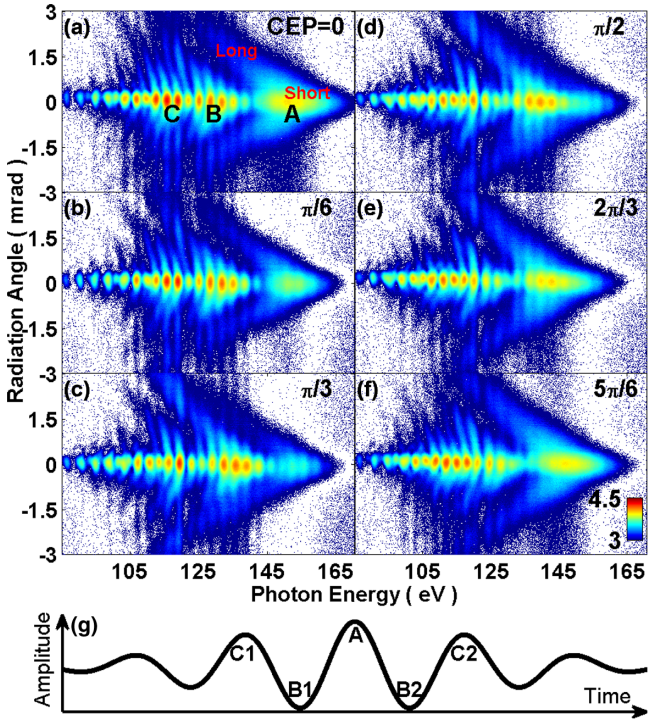

FIG. 1 (color online). (a)–(f) Experimental arrowlike high-harmonic spectra with different carrier envelope phase (CEP). (g) Schematic driven laser field when CEP = 0. All color bars are the same as that in (f), on a log scale.

harmonics have very different angular divergences and can be separated effectively at the far field. This is a general method that utilizes the laser phase to compensate the classical-like action and to control the final spatial distribution of high-order harmonics.

Our result is related to the previous theoretical work done by Chipperfield *et al.* [16]. They used few-cycle pulses and put a 2 mm gas cell behind the focus point, thereby obtaining a chevron-shaped harmonic spectrum, which mainly came from short trajectories and can directly link to individual electron trajectories. The structure was explained by phase matching, i.e., the propagation of harmonics in the gas cell. In our case, harmonics from both the short and long trajectories are simultaneously recorded, and more importantly are clearly resolved. The difference between these two trajectories leads to an arrowlike spectrum. The structure can be understood by the radial distribution of the total phase of harmonics in the generation slice.

Our experiment was carried out using carrier envelope phase (CEP) stabilized 4.2 fs pulses with energy of 0.4 mJ, wavelength of 800 nm, and repetition rate 1 kHz [17]. The gas cell was a sealed nickel tube of 1 mm diameter and was filled with neon gas. The laser pulse was focused by a spherical mirror with 0.4 m focus length into the gas cell to generate harmonics and a hole was drilled to let the harmonics go through. The gas pressure was around 20 kPa. The harmonics were focused by a toroidal mirror into an extreme ultraviolet spectrometer [18].

When the gas cell was located at about 3 mm in front of the focus point, an arrowlike harmonic spectrum was obtained, as shown in Fig. 1. The half-cycle cutoff structure provides us with an easy way to characterize the CEP of a driving pulse [12]. Figure 1(a) exhibits the spectrum when the CEP is close to 0, and Fig. 1(g) shows the corresponding schematic laser field. Harmonics from different half-cycles are separated along the axis of photon energy. Part *A* in Fig. 1(a) stands at the cutoff region and shows a continuous distribution, which comes from the most intense half-cycle of the driving pulse as seen at *A* in Fig. 1(g). Part *B* in Fig. 1(a) comes from the two half-cycles near the peak of the laser, shown as $B1$ and $B2$ in Fig. 1(g), and exhibits an interference pattern (discrete structure). Part *C* in Fig. 1(a) comes from even weaker half-cycles shown as $C1$ and $C2$ in Fig. 1(g). Harmonics from short trajectories form a long shaft on axis (radiation angle is 0), and the one from long trajectories form an arrowhead symmetric off axis. The two components separate in the direction of radiation angle, and together form an arrowlike shape. When the CEP varies, as shown in Figs. 1(b)—1(f), the pattern of the spectrum changes with the variation of the electric field under the pulse envelope; it clearly indicates that the connected off-axis and on-axis parts come from the same half-cycle. These characteristics show a full map from quantum trajectories to the high-harmonics spectrum.

The far-field spectrum is the Fourier transform of the harmonic's distribution in the generation region. The distribution can be expressed as two terms: the amplitude and the phase. We consider only a single slice with 0 thickness of the gas cell in the generation region. The fundamental laser is assumed to be a lowest-order Gaussian beam and propagates in the direction of positive z. The harmonic is assumed to have a Gaussian distribution of amplitude in the radial direction r.

The phase of the qth harmonic is $\phi_q(r,z) = -q\omega_0 t_r(r,z) + S_q(r,z)$ [6,19]. The first term can be expressed as the laser phase. The second term is the action of the electron accumulated in the continuum and can be expressed as $S_q(r,z) \approx \alpha_m I(r,z)$. ω_0 and $I(r,z)$ are the central angular frequency and the intensity of fundamental laser pulse, respectively. α is the coefficient of the intensity-dependent dipole phase [19,20], which is always negative, and $m = s, l$ represents short and long trajectories, respectively. If the action is expanded to the term of quadratic r and only r-related terms remain, the total phase can be written as

$$\phi_q(r,z) = c_{wz} r^2,$$
$$c_{wz} = \frac{qk}{2R_z} - 2\alpha_m \frac{I_{0z}}{w_z^2}, \quad (1)$$

where c_{wz} is the phase coefficient of the qth harmonic and determines how curved the wave front of the harmonic is. k is the wave vector. R_z, w_z, and I_{0z} are the radius of the wave front, the beam size, and the intensity on axis ($r = 0$), respectively, at z for the fundamental laser. The coefficient of the laser's quadratic phase, the first term in Eq. (1), changes from negative to positive when the value of z changes from $z < 0$ to $z > 0$. The coefficient of the action, the second term, is always positive. Compared to the case with the condition of $z > 0$ (behind the focus point), when the gas cell is located in the area of $z < 0$ (in front of the focus point), the coefficient c_{wz} is smaller and the corresponding harmonics have relatively small angular divergences. Especially for the short trajectory at a certain position, where $c_{wz} = 0$, the harmonic has a flat wave front and is a well-collimated beam. Because $|\alpha_l|$ is larger than $|\alpha_s|$, the harmonic from the long trajectory has a larger coefficient $|c_{wz}|$ and always has a larger angular divergence than that from the short trajectory [13,21,22]. The different divergences of the two trajectories can be qualitatively understood by the gradient of the total phase [23].

The amplitude of the qth harmonic can be expressed as $e^{-(r/w_{qz})^2}$. The size of the harmonic beam w_{qz} at the generation slice can be roughly estimated by the cutoff rule $\hbar\omega_{\text{cutoff}} = 3.17Up + I_p$ [24]. $\hbar$ is the reduced Plank constant, ω_{cutoff} is the angular frequency of the harmonic at cutoff, Up is the ponderomotive potential, and I_p is the ionization potential of the gas. The order of the harmonic is proportional to the intensity of laser linearly, so for the qth harmonic, the beam size at position z can be calculated as $w_{qz} = w_z\sqrt{(1/2)In(Q/q)}$, where Q is the order of the cutoff harmonic.

The phase and the amplitude together make the near-field distribution of the harmonic known. Fourier transform of the distribution gives the angular divergence of the harmonic:

$$\theta_q = \frac{\lambda_q}{2\pi w_{qz}}\sqrt{1 + c_{wz}^2 w_{qz}^2}, \tag{2}$$

where λ_q is the wavelength of the qth harmonic. When $z = 0$, $R_z = \infty$, so the laser phase in Eq. (1) vanishes and Eq. (2) degenerates to a simple expression [25].

The ratio of angular divergences of harmonics from the long trajectory to that of the short trajectory, as a function of the position of the gas cell, is defined as $R_{sl} = \theta_{ql}/\theta_{qs}$, and is shown in Fig. 2. For a certain photon energy, the beam sizes of harmonics from short and long trajectories are the same at the generation slice, so the difference of their angular divergences is determined only by their phase difference. When the gas cell is located in front of the focus point, the larger difference of the phases leads to the larger ratio. In particular, when the gas cell is around the position $z = -0.8z_R$, for nearly all the harmonics between 100 and 140 eV, as in Fig. 2, the ratios reach maximum. The larger

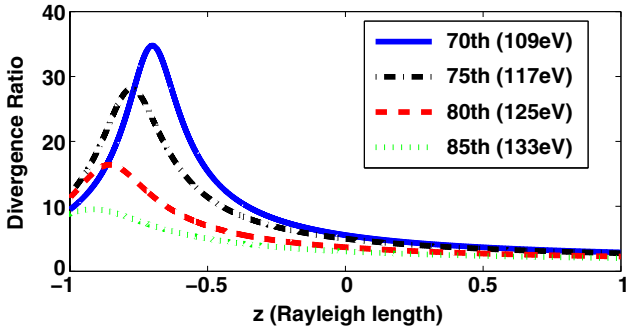

FIG. 2 (color online). Angular divergence ratio R_{sl} of harmonic from long trajectory to harmonic from short trajectory. The parameters of the laser beam are 800 nm, waist 60 μm, $I_{0z} = 6.65 \times 10^{14} W\ \text{cm}^{-2}$.

the difference of divergences, the less harmonics from short and long trajectories overlap each other in the direction of the radiation angle, and the more effectively the harmonics can be separated at the far field. So putting the gas cell in front of the focus point benefits the separation.

Our analytical model suggests that when putting the gas cell in front of the focus point, we can obtain a full quantum trajectories resolved high-harmonic spectrum. However, this model is based on multicycle pulses and assumes that the harmonic has a Gaussian spatial distribution of amplitude. To go beyond these approximations, we implemented numerical simulations, a one-dimensional soft-core time-dependent Schrödinger equation (TDSE) [26] for single-atom response, and a paraxial wave equation for propagation of harmonics [27,28]. Only one slice of the gas cell is considered, so the propagation is simplified to the Henkel transform. The spectra for different positions of the gas cell are shown in Fig. 3. When the gas cell is located in front of the focus point, harmonics from short trajectories are almost along the axis (radiation angle is 0) in Fig. 3(a) and are like a long shaft; harmonics from long trajectories are symmetric off axis in Fig. 3(b) and are like a arrowhead. Together they form an arrowlike structure in Fig. 3(c). When the gas cell moves towards the laser propagation direction, as in the right-hand column of Fig. 3, spatial distributions of the harmonics from both of the two trajectories become more divergent, closer, spatially overlapped, and form a chevron shape. In this case, harmonics from short and long trajectories cannot be effectively separated.

We have compared both the analytical results and TDSE simulations with experimental results. When the gas cell moves towards the laser propagation direction, the far-field harmonic spectrum changes from an arrowlike shape, as in Fig. 3(c), to a chevronlike shape, as in Fig. 3(f). The slope of the arrowhead also changes. Figure 4(a) shows a consistent change of the slope in both analytical and numerical models. The location of the gas cell in the experiment can be estimated by this calculation to be about

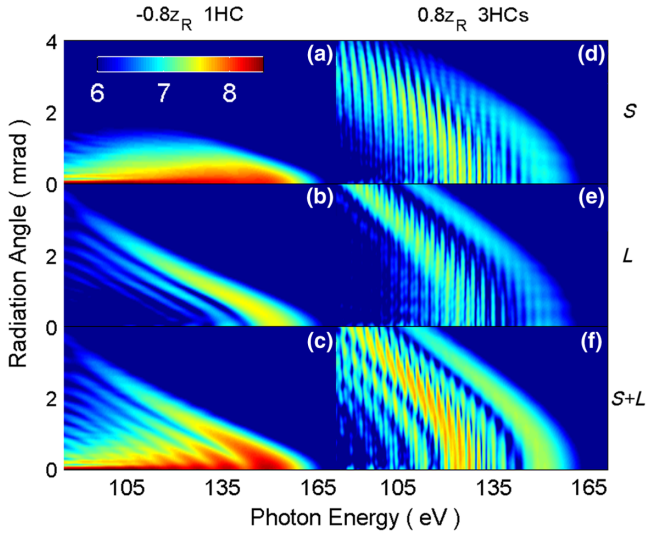

FIG. 3 (color online). Numerical far-field high-harmonic spectra. The target is located at 0.8 times the Rayleigh length (z_R) in front of the focus point (first column) and 0.8 times of z_R behind the focus point (second column). In the first column, the harmonics from the most intense half-cycle (HC) is calculated for the short (a), long (b), and both trajectories (c); in the second column, harmonics from three HCs are calculated for the short (d), long (e), and both trajectories (f). Pulse duration is 4.5 fs, other parameters are the same in Fig. 2. *S* and *L* are short and long trajectories. All color bars are the same as in (a), on a log scale.

0.3 times that of the Rayleigh length in front of the focus point. Figure 4(b) shows the corresponding divergences of harmonics from both short and long trajectories. The analytical model gives a similar arrowlike structure. The divergence of the harmonic for the short trajectory does not change much with harmonic order. On the contrary, for the long trajectory it decreases significantly. Finally, the two harmonics converge in the cutoff region. The TDSE simulation gives the more accurate and consistent results for the long trajectories, harmonics from which form the arrowhead in the spectrum.

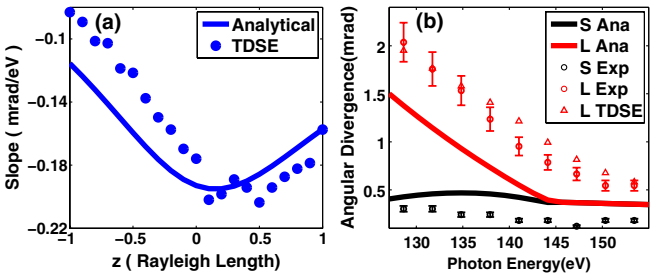

FIG. 4 (color online). (a) Slope of the arrowhead. (b) Angular divergences from short and long trajectories. *S* and *L* are short and long trajectories. Ana, Exp, and TDSE are analytical, experimental, and numerical results, respectively. Parameters of the laser are the same as in Fig. 2.

Figure 5 shows the comparison of the harmonics spectrum at the far field between the experiment and the simulation. Harmonics from the three most intense half-cycles for all trajectories are calculated. All of the features of the experimental spectrum are obtained from this calculation. This strongly supports our understanding that a full quantum trajectories resolved harmonic spectrum is recorded. It also supports the validity of our analytical model.

Although the length of the gas cell is 1 mm, the effective length of the interaction is probably far less than 1 mm for harmonics near the cutoff region; the phase mismatching effect is not obvious and the experimental harmonics mainly come from one slice in the generation region. The short length of interaction is also indicated by Haworth *et al.* [12] and Shiner *et al.* [29]. The arrowlike spectrum with the resolution of full quantum trajectories had survived from the phase mismatching effect. The survival is a key to obtaining information about the single-atom effect from the macrospectrum because it can be extracted only after not being washed out by the macroeffect. The phase matching for few-cycle pulses in HHG would be further investigated.

In conclusion, using few-cycle laser pulses we studied the variation of the two-dimensional high-order harmonics spectrum by changing the position of the gas cell relative to the focus point. Harmonics from the short and long quantum trajectories have different radial distributions of the total phase, so their angular divergences are different. When the gas cell is located in front of the focus point, the divergence difference can be maximal, so that the harmonics from the two trajectories can be effectively separated and form an arrowlike spectrum at the far field. At the same time, the relatively flat wave front makes the harmonic from the short trajectory almost collimated. The results directly give a full map of quantum trajectories in high-order harmonics generation.

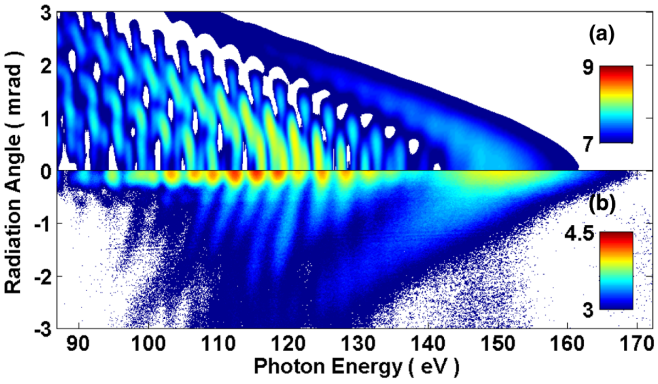

FIG. 5 (color online). Comparison between (a) numerical ($z = -0.3z_R$) and (b) experimental spectra, both on log scale. Parameters of the laser are the same as in Fig. 2.

The authors would like to thank John W. G. Tisch, Zenghu Chang, Mingyang Yu, and Binbin Wang for fruitful discussions. This work was partly supported by National Key Basic Research Program of China (No. 2013CB922401 and No. 2013CB922402), National Key Scientific Instrument and Equipment Development projects (No. 1012YQ12004704), National Natural Science Foundation of China (No. 11074298), and International Joint Research Program of National Natural Science Foundation of China (No. 61210017).

*hteng@iphy.ac.cn
†zywei@iphy.ac.cn

[1] P. M. Paul, E. S. Toma, P. Breger, G. Mullot, F. Auge, P. Balcou, H. G. Muller, and P. Agostini, Science **292**, 1689 (2001).
[2] M. Hentschel, R. Kienberger, C. Spielmann, G. Reider, N. Milosevic, T. Brabec, P. Corkum, U. Heinzmann, M. Drescher, and F. Krausz, Nature (London) **414**, 509 (2001).
[3] F. Krausz and M. Ivanov, Rev. Mod. Phys. **81**, 163 (2009).
[4] T. Popmintchev, M.-C. Chen, P. Arpin, M. M. Murnane, and H. C. Kapteyn, Nat. Photonics **4**, 822 (2010).
[5] P. B. Corkum, Phys. Rev. Lett. **71**, 1994 (1993).
[6] M. Lewenstein, P. Balcou, M. Y. Ivanov, A. L'Huillier, and P. B. Corkum, Phys. Rev. A **49**, 2117 (1994).
[7] R. P. Feynman and A. R. Hibbs, *Quantum Mechanics and Path Integrals* (McGraw-Hill, New York, 1965).
[8] P. Salières, B. Carré, L. Le Déroff, F. Grasbon, G. Paulus, H. Walther, R. Kopold, W. Becker, D. Milošević, A. Sanpera *et al.*, Science **292**, 902 (2001).
[9] J. Itatani, J. Levesque, D. Zeidler, H. Niikura, H. Pépin, J.-C. Kieffer, P. B. Corkum, and D. M. Villeneuve, Nature (London) **432**, 867 (2004).
[10] Y. Mairesse, J. Higuet, N. Dudovich, D. Shafir, B. Fabre, E. Mével, E. Constant, S. Patchkovskii, Z. Walters, M. Y. Ivanov, and O. Smirnova, Phys. Rev. Lett. **104**, 213601 (2010).
[11] A. Zair, T. Siegel, S. Sukiasyan, F. Risoud, L. Brugnera, C. Hutchison, Z. Diveki, T. Auguste, J. W. Tisch, P. Salires, M. Y. Ivanov, and J. P. Marangos, Chem. Phys. **414**, 184 (2013).
[12] C. Haworth, L. Chipperfield, J. Robinson, P. Knight, J. Marangos, and J. Tisch, Nat. Phys. **3**, 52 (2007).
[13] M. B. Gaarde, F. Salin, E. Constant, P. Balcou, K. J. Schafer, K. C. Kulander, and A. L'Huillier, Phys. Rev. A **59**, 1367 (1999).
[14] D. G. Lee, H. J. Shin, Y. H. Cha, K. H. Hong, J.-H. Kim, and C. H. Nam, Phys. Rev. A **63**, 021801 (2001).
[15] P. Salieres, A. L'Huillier, and M. Lewenstein, Phys. Rev. Lett. **74**, 3776 (1995).
[16] L. Chipperfield, P. Knight, J. Tisch, and J. Marangos, Opt. Commun. **264**, 494 (2006).
[17] W. Zhang, H. Teng, C.-X. Yun, P. Ye, M.-J. Zhan, S.-Y. Zhong, X.-K. He, L.-F. Wang, and Z.-Y. Wei, Chin. Phys. Lett. **31**, 084204 (2014).
[18] H. Teng, C.-X. Yun, X.-K. He, W. Zhang, L.-F. Wang, M.-J. Zhan, B.-b. Wang, and Z.-Y. Wei, Opt. Express **19**, 17 408 (2011).
[19] M. Lewenstein, P. Salières, and A. L'Huillier, Phys. Rev. A **52**, 4747 (1995).
[20] K. Varjú, Y. Mairesse, B. Carré, M. Gaarde, P. Johnsson, S. Kazamias, R. López-Martens, J. Mauritsson, K. Schafer, P. Balcou *et al.*, J. Mod. Opt. **52**, 379 (2005).
[21] M. Bellini, C. Lyngå, A. Tozzi, M. B. Gaarde, T. W. Hänsch, A. L'Huillier, and C.-G. Wahlström, Phys. Rev. Lett. **81**, 297 (1998).
[22] C. Lyngå, M. B. Gaarde, C. Delfin, M. Bellini, T. W. Hänsch, A. L'Huillier, and C.-G. Wahlström, Phys. Rev. A **60**, 4823 (1999).
[23] P. Balcou, P. Sali'eres, A. L'Huillier, and M. Lewenstein, Phys. Rev. A **55**, 3204 (1997).
[24] A. L'Huillier, M. Lewenstein, P. Salières, P. Balcou, M. Y. Ivanov, J. Larsson, and C. G. Wahlström, Phys. Rev. A **48**, R3433 (1993).
[25] X. He, M. Miranda, J. Schwenke, O. Guilbaud, T. Ruchon, C. Heyl, E. Georgadiou, R. Rakowski, A. Persson, M. B. Gaarde, and A. L'Huillier, Phys. Rev. A **79**, 063829 (2009).
[26] M. Feit, J. Fleck, Jr., and A. Steiger, J. Comput. Phys. **47**, 412 (1982).
[27] A. E. Siegman, *Lasers* (University Science Books, Mill Valley, CA, 1986), p. 661.
[28] J. Muffett, C.-G. Wahlstrom, and M. Hutchinson, J. Phys. B **27**, 5693 (1994).
[29] A. Shiner, B. Schmidt, C. Trallero-Herrero, H. Wörner, S. Patchkovskii, P. Corkum, J. Kieffer, F. Légaré, and D. Villeneuve, Nat. Phys. **7**, 464 (2011).